



Erosion Performance of HVOF-Sprayed $\text{Cr}_3\text{C}_2\text{-NiCr}$ Coatings

Gang-Chang Ji, Chang-Jiu Li, Yu-Yue Wang, and Wen-Ya Li

(Submitted October 1, 2006; in revised form March 21, 2007)

$\text{Cr}_3\text{C}_2\text{-NiCr}$ coatings were deposited by high-velocity oxygen fuel (HVOF) spraying process under spray conditions of different flows of oxygen and propane gases, and spray distances. The orthogonal regression experimental design method was used for systematic investigation of the influence of spray parameters on the erosion performance of $\text{Cr}_3\text{C}_2\text{-NiCr}$ coatings. Erosion tests were performed at different jet angles of abrasive particles. The erosion mechanism of $\text{Cr}_3\text{C}_2\text{-NiCr}$ coatings was examined through the surface morphology and cross-sectional microstructure of the eroded coatings. The correlations of the carbide particle size and carbide content with the erosion rate were examined. It was found that the erosion occurred dominantly by spalling of splats from the lamellar interfaces. The spalling resulted from the propagation of cracks parallel to the interfaces between the lamellae exposed to the surface and underlying coating. The carbide particle size and content in the coating influenced significantly the erosion performance of $\text{Cr}_3\text{C}_2\text{-NiCr}$ coatings.

Keywords $\text{Cr}_3\text{C}_2\text{-NiCr}$ coatings, erosion mechanisms, erosion performance, high-velocity oxygen fuel (HVOF)

1. Introduction

Chromium carbide coatings are widely applied to the parts subjected to high-temperature wear and erosion (Ref 1-11). It is usually considered that the wear and erosion resistance of cermet coatings are predominately influenced by its microstructures including the splat size, carbide particle size, carbide content and carbide distribution within a splat, and the cohesion between the splats (Ref 11-14). On the other hand, the microstructure of high-velocity oxygen fuel (HVOF)-sprayed cermet coatings is significantly influenced by the microstructure of starting powder, spray system, and spray conditions (Ref 15-22). Previous studies suggested that the coatings with a higher amount of fine carbides embedded exhibit a better wear performance (Ref 13, 14). Recently, HVOF spray process is preferably used to deposit cermet coatings such as $\text{Cr}_3\text{C}_2\text{-NiCr}$, WC-Co, etc. This is because the coatings deposited by the HVOF process exhibit high density, low porosity, and excellent adhesive strength with much more carbide particles retained in the matrix of the cermet compared with plasma spraying process (Ref 15, 17).

Gang-Chang Ji, School of Materials Science and Engineering, Jiujiang University, 551, Qianjin East Road, Jiujiang 332005, Jiangxi, China; **Chang-Jiu Li** and **Yu-Yue Wang**, State Key Laboratory for Mechanical Behavior of Materials, School of Materials Science and Engineering, Xi'an Jiaotong University, Xi'an 710049, China; and **Wen-Ya Li**, Shaanxi Key Laboratory of Friction Welding Technologies, Northwestern Polytechnical University, Xi'an 710072, China. Contact e-mail: jigg@jjtu.edu.cn.

In HVOF process, however, the coating microstructure, which dominates the wear performance of the coatings, is significantly influenced by starting materials (Ref 12-14), spray systems (Ref 15, 16), and spray parameters including flows of oxygen and fuel gases and spray distances (Ref 17-19). Therefore, many studies have been conducted to optimize the compositions of starting materials and the spray conditions of HVOF $\text{Cr}_3\text{C}_2\text{-NiCr}$ coatings for anti-wear and anti-erosion applications (Ref 12-17). Since different HVOF systems have different operating parameters and different parameter ranges, it is essential to understand the main microstructural features which control the erosion of coatings and mechanisms of erosion. Furthermore, the understanding of correlations between the spray parameters and coating microstructure will benefit the optimization of coating erosion performance. Although many papers were involved in the investigation of erosion of $\text{Cr}_3\text{C}_2\text{-NiCr}$ coatings, the erosion mechanisms of HVOF $\text{Cr}_3\text{C}_2\text{-NiCr}$ coatings were still insufficiently understood.

The purpose of this paper is to examine the erosion behavior and mechanism of HVOF-sprayed $\text{Cr}_3\text{C}_2\text{-NiCr}$ coatings through investigating systematically the effects of spray parameters including fuel gas flow, oxygen flow, and spray distance on the erosion performance based on the orthogonal regression experimental design method. The correlations between hard carbide phase and erosion rate were also examined to reveal its effect on the erosion of the coatings.

2. Materials and Experimental Procedure

2.1 Materials

Commercially available sinter-crushed $\text{Cr}_3\text{C}_2\text{-25 wt.}\% \text{NiCr}$ powder with a particle size range of 10–55 μm was used in this experiment. The powder

exhibited an angular shape as shown in Fig. 1. Mild steel plates of dimensions of $50 \times 60 \times 4.5$ mm were used as substrates which were sand-blasted using 20-mesh alumina grits before spraying.

2.2 Coating Deposition

Cr_3C_2 -NiCr coatings were prepared using the HVOF spray system (CH-2000) developed in Xi'an Jiaotong University. A detailed description of the system can be found elsewhere (Ref 23). Propane and nitrogen gases were used as fuel and powder carrier gases, respectively. The flows of oxygen and propane, and spray distance were changed in five levels according to the orthogonal experimental design. The values of parameters corresponding to each level are given in Table 1. The pressures of propane, oxygen, and nitrogen were fixed at 0.4, 0.55, and 0.35 MPa during spraying, respectively. The detailed experimental conditions are shown in Table 2.

2.3 Characterization of Microstructure

Microstructures of the starting powder and coating and morphologies of the eroded coating surfaces were examined by scanning electron microscopy (SEM). The thickness of as-sprayed coatings was in the range of 200–300 μm . The mean particle size and volume fraction of carbides in the as-sprayed coatings were measured from the cross-sectional SEM micrographs through an image analysis method. The porosity of coatings was estimated from the density difference between the ideal and actual

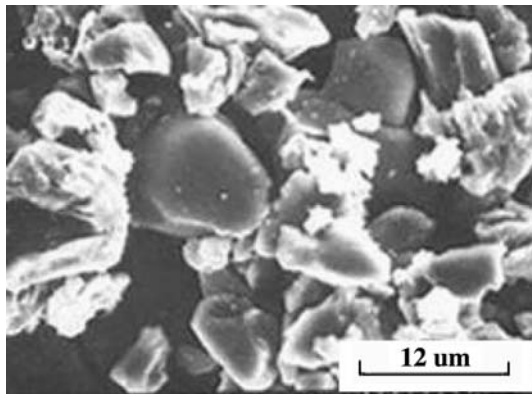


Fig. 1 Morphology of the Cr_3C_2 -25wt.%NiCr powder

Table 1 Spray parameter levels and values

Mark of level	O_2 flow, L/min	C_3H_8 , L/min	S.D., mm
+r	526	45.8	258.6
+1	510	44.3	250
0	447	37	210
-1	382	29.6	170
-r	368	28.1	161.4

S.D.: Spray distance

coatings. The actual density was evaluated by the weight and volume of a sample. The theoretical density of the coating was calculated using the densities of the constituents of ideal coating without porosity according to the calculation method for composites.

2.4 Erosion Test

Erosion resistance of Cr_3C_2 -NiCr coating was tested by a blast erosion tester as shown schematically in Fig. 2. A compressed air was used as an accelerating gas of erosive particles. In this tester, an accelerating nozzle has a diameter of 3.6 mm and a length of 22 mm. The pressure and flow rate of the compressed air were fixed to 0.35 MPa and 141 L/min. 60-mesh alumina grits with a microhardness ($\text{Hv}_{0.1}$) of 1940 kgf/mm^2 were used as the abrasives. The jet angles (α in Fig. 2) of erosive particles with respect

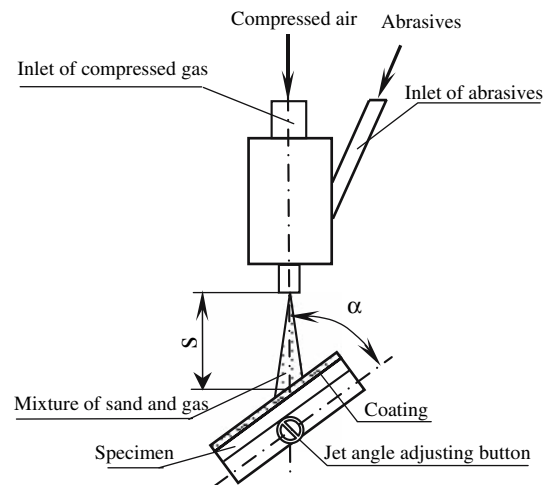


Fig. 2 Schematic of the erosion tester

Table 2 Arrangement of parameter levels and experimental results

Exp. No.	Levels			Erosion rate, mg/g		$\text{Hv}_{0.3}$, kgf/mm^2
	O_2	C_3H_8	S.D.	Y_{el}	Y_{ev}	
1	1	1	1	0.625	0.978	814
2	1	1	-1	0.613	1.545	868
3	1	-1	1	0.688	1.40	598
4	1	-1	-1	0.603	1.115	705
5	-1	1	1	0.528	0.938	745
6	-1	1	-1	0.528	1.138	891
7	-1	-1	1	0.555	1.223	576
8	-1	-1	-1	0.585	1.258	583
9	r	0	0	0.585	1.203	610
10	-r	0	0	0.50	1.218	719
11	0	r	0	0.49	1.148	763
12	0	-r	0	0.545	0.995	581
13	0	0	r	0.558	1.04	535
14	0	0	-r	0.48	0.988	661
15	0	0	0	0.49	0.905	723

Y_{el} : Erosion rate at 30° ; Y_{ev} : erosion rate at 90°

to coating surface were changed from 30° to 90°. The distance from the nozzle exit to the center of sample surface was 100 mm to permit all erosive particles impacting on coating surface. The erosion test was performed successively with 20 g abrasives at one test and the coating weight loss was measured after each test. The erosion rate was estimated based on the linear relation between the weight loss of the coatings and the weight of the abrasives used at a stable erosion state, and determined by the average value of ten tests.

3. Results and Discussion

3.1 Microstructures of the Starting Powder and Coating

It was clearly shown in Fig. 1 that the powder particles used in the present study had an angular shape. Examination of cross-sectional microstructure of powder revealed that the powder particle had a dense microstructure with small angular Cr_3C_2 particles aggregated by NiCr alloy matrix, as shown in Fig. 3. The mean carbide size in the starting powder is about 6.4 μm . Figure 4 shows a typical cross-sectional microstructure of HVOF-sprayed Cr_3C_2 -NiCr coating. It can be found that the coating exhibits a typical lamellar structure which is formed by the stacking of splats elongated in the direction parallel to substrate surface. Most carbide particles within the as-sprayed coating still presented an angular shape and the NiCr binder phase was composed of complex phases, such as amorphous phase, nanocrystallines, and microcrystallines which were revealed by transmission electron microscopy examination as reported elsewhere (Ref 24). The porosities of all coatings estimated from density difference were less than 1.0%.

3.2 Erosion of HVOF Cr_3C_2 Coatings

Figure 5 shows a typical erosion test result representing the change of the coating weight loss with increasing number of test. It was found that the coating weight loss

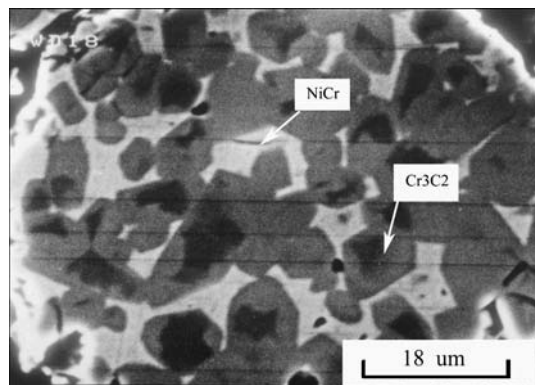


Fig. 3 Cross-sectional microstructure of the Cr_3C_2 -25wt.%NiCr powder

almost increased linearly with the increase of abrasive weight under a jet angle of 90°. A linear relation between coating weight loss and abrasive weight used was observed. When the test was performed at a jet angle of 30°, the similar linear relation was achieved after erosion using about 40 g abrasives. The erosion rates (Y_{ew}) at individual jet angles were obtained from the slopes of the linear relation between weight loss of the coatings and the weight of abrasives.

Figure 6 shows effect of jet angle on the erosion rate for the coatings deposited under conditions from No. 9 to 15 as shown in Table 2. It can be found that the erosion rate increased with the increase of jet angle of erosive particles. Under 90° impact the erosion rate reached to a maximum value for all coatings. Such characteristic was typical for thermally sprayed ceramic coatings (Ref 25). This fact implies that the erosion of HVOF Cr_3C_2 coating presents a behavior similar to that of brittle materials (Ref 26).

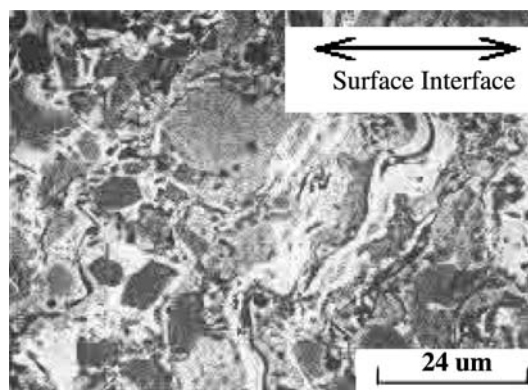


Fig. 4 Typical cross-sectional structure of HVOF Cr_3C_2 -NiCr coating

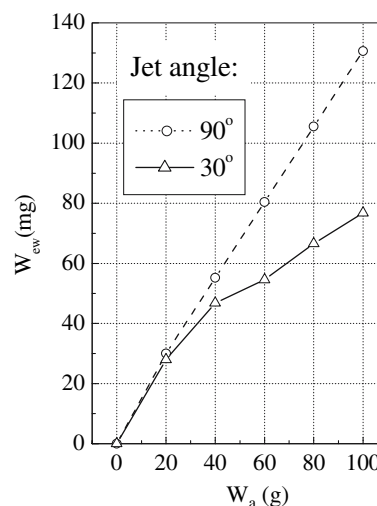


Fig. 5 Change of coating weight loss (W_{ew}) with weight of abrasives (W_a)

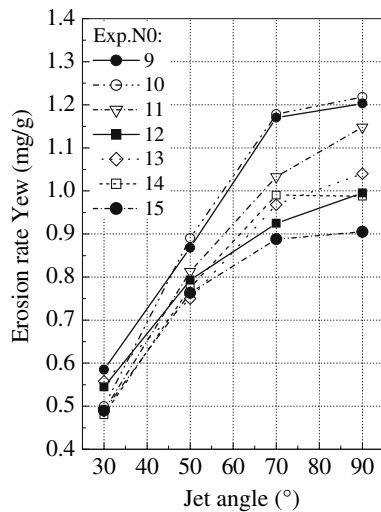


Fig. 6 Effect of jet angle of abrasive particles on erosion rate of HVOF $\text{Cr}_3\text{C}_2\text{-NiCr}$ coatings

For all coatings deposited using spray conditions as shown in Table 1, the erosion rates at both 30° and 90° were measured. The results were shown in Table 2. Those results clearly revealed that erosion rate of HVOF $\text{Cr}_3\text{C}_2\text{-NiCr}$ coating was significantly influenced by spray parameters. However, it was also found that the effect of individual spray parameters on erosion rate was complicated owing to the intereffect of spray parameters. To examine the effects of individual spray parameters, the following regression formulae for 30° and 90° were obtained based on the experimental data (Ref 19).

$$Y_{el} = 490.2 - 1.17X_1 - 4.64X_2 - 1.04X_3 + 0.000824X_1X_2 + 0.00062X_1X_3 - 0.00183X_2X_3 + 0.0012X_1^2 + 0.0596X_2^2 + 0.00208X_3^2 \quad (\text{Eq 1})$$

$$Y_{ev} = 945.4 - 3.79X_1 - 4.89X_2 + 0.825X_3 + 0.011X_1X_2 - 0.0432X_2X_3 + 0.00387X_1^2 + 0.119X_2^2 + 0.00159X_3^2 \quad (\text{Eq 2})$$

where X_1 , X_2 , and X_3 are oxygen flow, propane flow, and spray distance, respectively. Y_{el} and Y_{ev} are the erosion rate at 30° and 90° , respectively. By use of those formulae, the effects of spray parameters on erosion rate of the coating can be systematically examined as follows.

3.3 Effect of Spray Parameters on the Erosion at 30°

Figures 7, 8, and 9 show the influences of propane flow, oxygen flow, and spray distance on erosion rate of the coatings at a jet angle of 30° , respectively. Those results were calculated from the orthogonal regression formula (Eq 1). It can be found that the variations of the erosion rate with the flows of both propane and oxygen follow a concave curve. The coatings with a comparatively lower erosion rate can be deposited using moderate flows of oxygen and propane. It is evident from Fig. 9 that with an

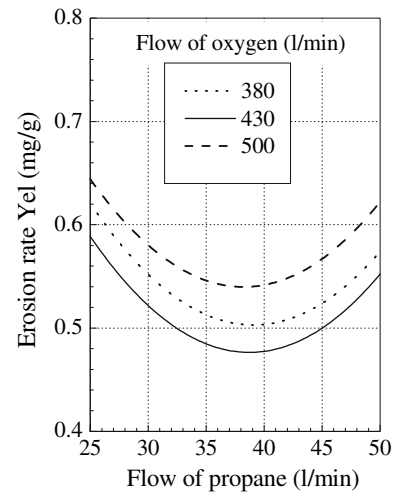


Fig. 7 Effect of propane flow on erosion rate of $\text{Cr}_3\text{C}_2\text{-NiCr}$ coating at jet angle of 30° . Spray distance: 180 mm

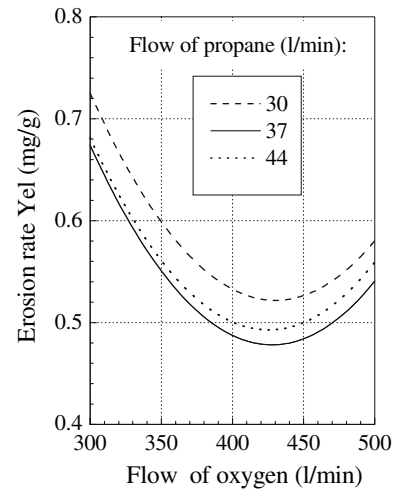


Fig. 8 Effect of oxygen flow on erosion rate of $\text{Cr}_3\text{C}_2\text{-NiCr}$ coating at jet angle of 30° . Spray distance: 180 mm

increase in spray distance the erosion rate decreases first and then tends to increase significantly when spray distance increases to about 240 mm.

3.4 Effect of Spray Parameters on the Erosion at 90°

Figures 10, 11, and 12 show the influences of propane flow, oxygen flow, and spray distance on erosion rates of the coating at a jet angle of 90° , respectively. It can be found from Fig. 10 that propane flow influences less significantly the erosion of the coating with the increase of propane flow up to about 35 L/min although the erosion rate shows a decreasing tendency. However, the erosion rate tends to increase with a further increment of propane flow. From Fig. 11 it can be recognized that the erosion rate of the coating is decreased when oxygen flow increases

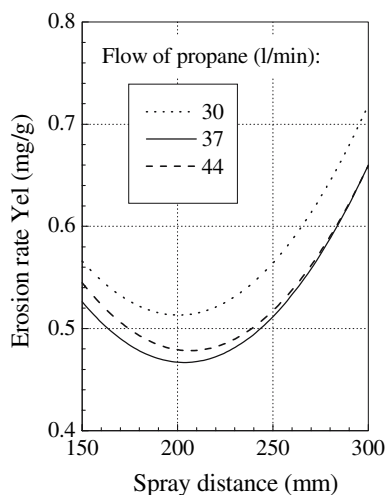


Fig. 9 Effect of spray distance on erosion rate of $\text{Cr}_3\text{C}_2\text{-NiCr}$ coating at jet angle of 30° . Flow of oxygen: 430 L/min

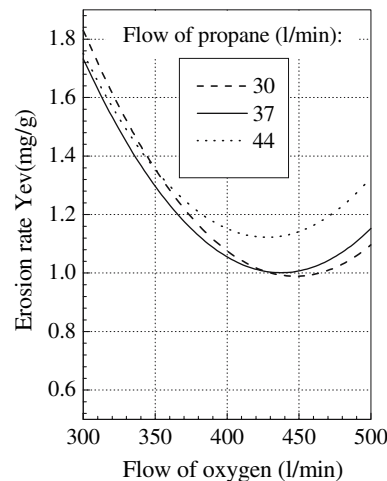


Fig. 11 Effect of oxygen flow on erosion rate of $\text{Cr}_3\text{C}_2\text{-NiCr}$ coating at jet angle of 90° . Spray distance: 180 mm

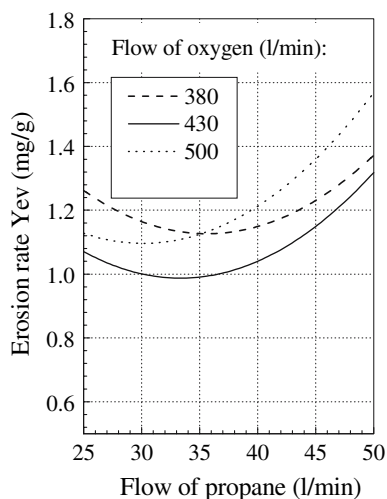


Fig. 10 Effect of propane flow on erosion rate of $\text{Cr}_3\text{C}_2\text{-NiCr}$ coating at jet angle of 90° . Spray distance: 180 mm

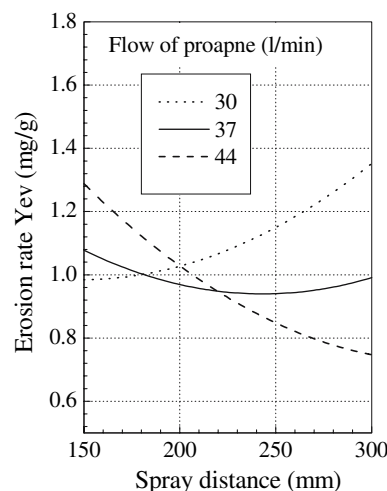


Fig. 12 Effect of spray distance on erosion rate of $\text{Cr}_3\text{C}_2\text{-NiCr}$ coating at jet angle of 90° . Flow of oxygen: 430 L/min

from 300 to 400 L/min. However, when the flow of oxygen exceeds about 400 L/min, the further increase of oxygen flow presents a comparatively less effect on the erosion rate and the erosion rate increases slightly with the increment of oxygen flow. Figure 12 shows clearly that the effect of spray distance on the erosion rate depends on the other spray parameters. When propane flow is 44 L/min, the erosion rate of the coating decreases with the increase of spray distance. On the contrary, when propane flow is at about 30 L/min, the increase of spray distance leads to the increase of the erosion rate. Moreover, it is found that when propane flow is at around 37 L/min, the erosion rate is not significantly influenced by spray distance. Through a close examination of the results indicated by Fig. 10 to 12, it can be found that the flows of oxygen and propane, and spray distance have certain intereffect on erosion performance, especially with propane flow and spray distance.

Those relations between the erosion rate and HVOF spray parameters have also been confirmed by the other $\text{Cr}_3\text{C}_2\text{-NiCr}$ coatings deposited by the other type of powders and by different HVOF systems (Ref 27).

3.5 Erosion Mechanisms

Figure 13 shows a typical morphology of the coating surface and cross-section after erosion test at 90° . From the cross-sectional microstructure (Fig. 13a), substantial cracks along the interface between the lamellar layer exposed to coating surface and subsurface lamellar layers were observed. It can be considered that such cracks initiate from the nonbonded lamellar interface area and propagate along the lamellar interfaces under impact of abrasives owing to relatively limited weak bonding. The lamellar interfaces in a thermally sprayed ceramic coatings

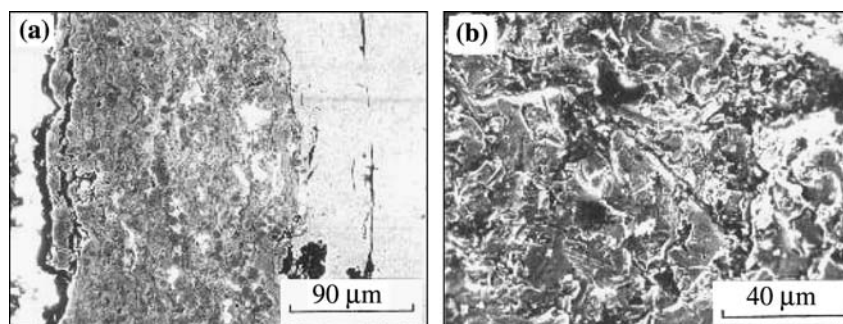


Fig. 13 Erosion morphology of $\text{Cr}_3\text{C}_2\text{-NiCr}$ coating at 90° . (a) cross section and (b) surface

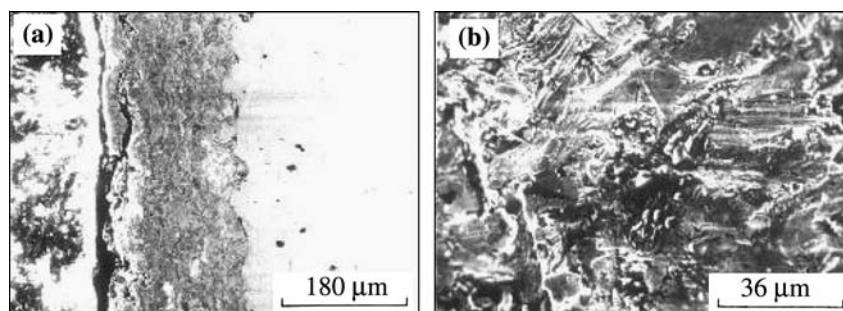


Fig. 14 Erosion morphology of $\text{Cr}_3\text{C}_2\text{-NiCr}$ coating at 30° . (a) cross section and (b) surface

are only partially bonded together with over one-third of the interfaces nonbonded (Ref 28, 29). The growth of these cracks throughout whole interface area finally leads to spalling of lamellae, which are exposed on coating surface and subjected to direct impact of abrasives. Meanwhile, the morphology examination of coating surface after erosion showed that there also existed the evidence of ploughing.

Figure 14 shows the morphology of the coating surface and the microstructure of cross section of the sample eroded at 30° . It can be observed that there are small craters on the eroded surface formed by the peeling off of carbides within matrix (Fig. 14b) and some narrow gouges as well. Meanwhile, the chips and pits were evidently found from cross section of the sample (Fig. 14a). This result implies that the erosion of the coating occurs through spalling of lamella owing to propagation of cracks along lamellar interfaces and ploughing of NiCr matrix by abrasives. The morphology examination of the eroded surface also showed that the ploughing became more evident with the decrease of jet angle of erosive particles. However, taking the dependency of erosion rate on impact angle into account, it can be considered that the dominant erosion of HVOF-sprayed $\text{Cr}_3\text{C}_2\text{-NiCr}$ coating occurs through lamella spalling.

Therefore, examination of cross sections and surfaces of eroded coating suggests that the erosion of HVOF-sprayed $\text{Cr}_3\text{C}_2\text{-NiCr}$ coating occurs through two mechanisms. The first one is microcutting and ploughing of soft

binder matrix by hard abrasives. With progress of erosion, the harder carbide particles are exposed and then gouged out by further impact of abrasive particles, which leads to further removal of the matrix by cutting. This appears to be a less-dominated mechanism, especially at high impact angle.

The second one is lamella spalling resulting from cracks propagation as shown in Fig. 15. The study of interlamellar bonding has revealed that only less than one-third interface area is bonded together in plasma-sprayed ceramic coatings (Ref 28, 29), while two-third interface area between lamellae exists as interlamellar gaps which can be considered as pre-existing cracks as well. Although there is no any interface bonding data available for cermet coating deposited by HVOF process, it may be reasonable to consider HVOF cermet coating having a lamellar bonding state comparable to plasma-sprayed ceramic coating. This is because the lamellar bonding ratio of an alumina coating deposited by detonation gun spray, which is characterized as typical high-velocity spray process, was lower than the plasma-sprayed coating (Ref 30). Therefore, there could be substantial pre-cracks between lamellae interfaces as shown in Fig. 15a. Under impact of abrasive particles, the propagation of pre-cracks in the form of lamellar interface gap occurs easily along lamellar interface (Fig. 15b). Once these cracks interlink through pre-existing non-bonded interface areas throughout the whole lamellae interface, either a mono lamella or multi-lamellae removal occurs (Fig. 15c).

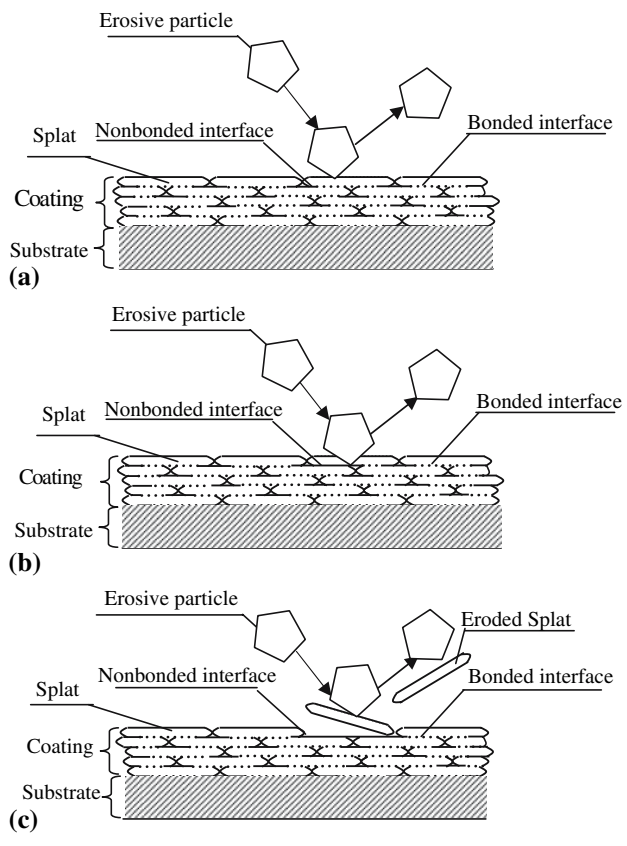


Fig. 15 Schematic of erosion behavior of $\text{Cr}_3\text{C}_2\text{-NiCr}$ coating

Under the erosion at 90° , the contribution of the microcutting to erosion will be limited. In the case that single lamella spalling is a dominant erosion process, the erosion rate of the coating will be inversely related to the cohesion between splats and positively related to lamella thickness (Ref 31, 32). During deposition of cermet coating by HVOF, lamella thickness depends directly on solid carbide particle size (Ref 14, 18). Moreover, the higher carbide content in lamella is associated with a more limited spreading of lamella during splatting, which results in generation of more concentrated impact contact pressure (Ref 33). As a result, it can be considered that the improved cohesion between lamellae may be achieved with a lamella of higher carbide content. Figure 16 shows the effect of the ratio of mean carbide particle size to carbide fraction on erosion rate at 90° . Both the mean carbide particle size and carbide volume fraction were measured from cross-sectional microstructure of the coatings. It is evident that with the increase of the ratio the erosion rate tends to increase. The result suggests that the coating with less carbide content and large mean carbide particle size will be eroded at a high erosion rate. This is because both large carbide particles increase lamella thickness and retention of high carbide content during solid-liquid two-phase droplet may enhance the cohesion between lamellae (Ref 34).

On the other hand, the examination into the effect of carbide content reveals that the carbide content in the

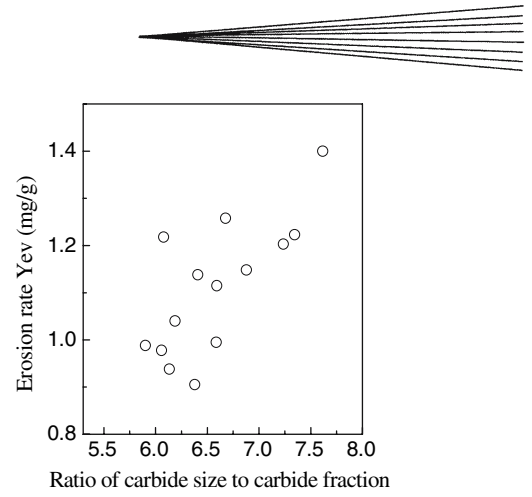


Fig. 16 Effect of the ratio of mean carbide size to carbide content on the erosion rate at 90°

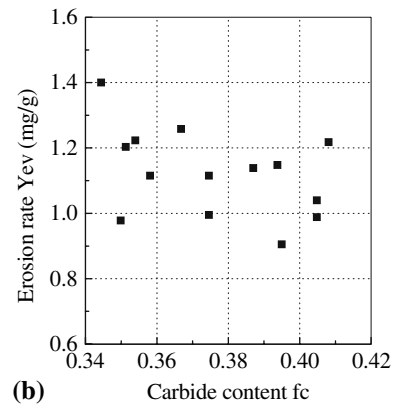
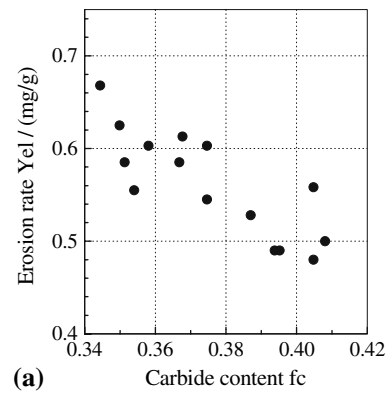


Fig. 17 Effect of carbide content on the erosion rate at (a) 30° and (b) 90°

coating exhibits influence on the erosion rate at 30° and 90° as shown in Fig. 17(a) and (b), respectively. It is clear that with the increase of carbide content in the coating the erosion rate decreases. This is because increasing carbide content enhanced the ability of the coating to resist cutting wear and cohesion between lamellae as well. Moreover, it is obvious that the influence of carbide content on erosion performance is more significant at 30° than 90° . Therefore, at low impact angle the microcutting may contribute

significantly to the erosion, although splat spalling was evidently observed as shown by Fig. 14. As the jet impact angle increase, the action of vertical momentum of erosive particles will increase. Consequently, the erosion of the coating will be changed from microcutting-ploughing and lamella spalling mechanisms to lamella spalling-controlled mechanisms.

The above results exhibit that erosion performance of cermet coating is influenced by spray parameters through carbide content and size. The previous study showed that the rebounding off of large carbide particles is mainly responsible for carbon loss during HVOF of $\text{Cr}_3\text{C}_2\text{-NiCr}$ (Ref 35). The well melting of spray particles results in thin splats and subsequent easy rebound-off of carbide particles (Ref 14). Therefore, it can be considered that the spray conditions under which melting and velocity of spray particle is improved tends to deteriorate erosion performance of HVOF $\text{Cr}_3\text{C}_2\text{-NiCr}$ coating through decreasing carbide content. On the other hand, the preferable rebounding off of large carbides tends to decrease mean carbide particle size, which may enhance the erosion performance of the coating.

Since the tendency of rebounding-off of solid carbide particle on droplet impact increases with carbide particle size (Ref 14-18), the high carbide content can be easily obtained by spray particles of small size of carbide (Ref 17). Therefore, it can be considered that deposition of $\text{Cr}_3\text{C}_2\text{-NiCr}$ coatings using feedstocks of small carbide particles aggregated densely can contribute to a high carbide retention and also small carbide particle size, and consequently an improved erosion performance of HVOF $\text{Cr}_3\text{C}_2\text{-NiCr}$ coatings.

4. Conclusions

The effect of spray parameters on the erosion performance of HVOF-deposited $\text{Cr}_3\text{C}_2\text{-NiCr}$ coatings was systematically investigated using the orthogonal regression experimental design method. The erosion mechanism of the coating was examined through the cross-sectional microstructure and surface morphology of the eroded coating. It was clear that the erosion rate of $\text{Cr}_3\text{C}_2\text{-NiCr}$ coatings increased with increase of the abrasive impact angle and reached to a maximum value at 90° . The erosion performance of $\text{Cr}_3\text{C}_2\text{-NiCr}$ coatings was significantly influenced by the flows of both propane and oxygen gases. The effect of spray distance on the erosion rate depended on flows of propane and oxygen. The spalling-off of lamellae from the interlamellar interface was mainly responsible for the erosion of HVOF $\text{Cr}_3\text{C}_2\text{-NiCr}$ coatings at relatively high erosion angles. The micro-cutting, gouging, and carbide peeling out occurred in a low-angle erosion besides lamellae spalling. The size and content of carbide particles in the coatings significantly influenced the erosion behavior. The small carbide particles may lead to reduction of lamella thickness and consequently an improved erosion performance. Therefore, it is considered that the erosion performance of HVOF $\text{Cr}_3\text{C}_2\text{-NiCr}$

coating may be improved by using feedstock of small size of carbides.

Acknowledgments

This work is partially supported by the Natural Science Foundation of Jiangxi Province and Science and Technology Project of Jiangxi Educational Bureau.

References

1. Y. Fukuda, H. Yamasaki, M. Kawahara, and H. Kimura, Detonation Coating for Coal Fired Tubes, *Proceedings of International Symposium on Advanced Thermal Spray Technology and Applied Coating*, Japan High Temperature Society, Osaka, 1988, p 49-54
2. H. Fukutome, H. Shimizu, N. Yamashita, and Y. Shimizu, The Application of Cermet Coating on Piston Ring by HVOF. Proceedings of 14th International Thermal Spray Conference, A. Ohmori, Ed., Osaka: Japan High Temperature Society, 1995, p 21-26
3. B.Q. Wang, G.Q. Geng, A.V. Levy, and E.R. Buchanan, Elevated Temperature Erosion of Carbide-Metal Composite. Proceedings of the International Thermal Spray Conference and Exposition, C.C. Berndt, Ed., Materials Park, OH, USA: ASM International, 1992, p 735-742
4. P. Sahoo and R. Raghuraman, Chromium Carbide Reinforced Composite Coatings for High Temperature Hard-Coat Applications. *Thermal Spray Coatings: Research, Design and Applications*, C.C. Berndt and T.F. Bernecki, Eds., Materials Park, OH, USA: ASM International, 1993, p 405-410
5. B.Q. Wang and K. Luer, The Erosion-Oxidation Behavior of HVOF $\text{Cr}_3\text{C}_2\text{-NiCr}$ Cermet Coating, *Wear*, 1994, **174**, p 177-185
6. E. Lugscheider, P. Remer, C. Herbst, and K. Yushchenko, et al., NiCr- Cr_3C_2 and NiCr-TiC High Wear Resistant Coatings for Protective Applications in Steam Turbines. Proceedings of 14th International Thermal Spray Conference, A. Ohmori, Ed., Osaka: Japan High Temperature Society, 1995, p 235-240
7. B.Q. Wang, The Erosion-Corrosion Behavior of Thermal Sprayed Coatings in Fluidized Bed Combustor Systems. *Surface Modification Technology X*, T.S. Sudarshan, K.A. Khor, and M. Jeandin, Eds., London: The Institute of Materials, 1996, p 265-277
8. I. Fagoaga, J.L. Viviente, P. Gavin, J.M. Bronte, J. Garcia, and J.A. Tagle, Multilayer Coatings by Continuous Detonation System Spray Technique, *Thin Solid Films*, 1998, **317**, p 259-265
9. B.S. Mann and B. Prakash, High Temperature Friction and Wear Characteristics of Various Coating Materials for Steam Valve Spindle Application, *Wear*, 2000, **240**, p 223-230
10. B.G. Seong, S.Y. Hwang, and K.Y. Kim, High Temperature Corrosion of Recuperation Used in Steel Mills, *Surf. Coat. Technol.*, 2000, **126**, p 256-265
11. B.Q. Wang and Z.R. Shui, The Hot Erosion Behavior of HVOF Chromium Carbide-Metal Cermet Coatings Sprayed with Different Powders, *Wear*, 2002, **253**, p 550-557
12. K.J. Stein, B.S. Schorr, and A.R. Marder, Erosion of Thermal Spray MCr- Cr_3C_2 Cermet Coatings, *Wear*, 1999, **224**, p 153-159
13. C.-J. Li, A. Ohmori, and K. Tani, Effect of WC Particle Size on the Abrasive Wear of Thermally Sprayed WC-Co Coatings, *Mater. Manuf. Process.*, 1999, **14**, p 175-184
14. C.-J. Li, Y.-Y. Wang, G.-J. Yang, A. Ohmori, and K.A. Khor, Effect of Solid Carbide Particle Size on Deposition Behavior, Microstructure and Wear Performance of HVOF Cermet Coatings, *Mater. Sci. Technol.*, 2004, **20**, p 1087-1096
15. P. Vuoristo, K. Niemi, A. Makela, and T. Mantyla, Abrasion and Erosion of Wear Resistance of $\text{Cr}_3\text{C}_2\text{-NiCr}$ Coatings Prepared Plasma, Detonation and High Velocity Oxy-Fuel Spraying. *Thermal Spray Industrial Applications*, C.C. Berndt and S. Sampath, Eds., Materials Park, OH, USA: ASM International, 1994, p 121-126



16. S. Zimmermann and H. Kreye, Chromium Carbide Coatings Produced by Various HVOF Spray Systems. *Thermal Spray: Practical Solutions for Engineering Problems*, C.C. Berndt, Ed., Materials Park, OH: ASM International, 1996, p 147-152
17. C.-J. Li, A. Ohmori, and Y. Harada, Effect of WC-Co Powder Structure on the Structure of Thermally Sprayed WC-Co Coatings, *J. Mater. Sci.*, 1996, **31**, p 785-794
18. C.-J. Li, G.-C. Ji, Y.-Y. Wang, and K. Sonoya, The Dominant Mechanism of Carbon Loss During HVOF Spraying of Cr₃C₂-NiCr, *Thin Solid Films*, 2002, **419**, p 137-143
19. C.-J. Li, K. Sonoya, G.-C. Ji, and Y.-Y. Wang, Effect of Spray Conditions on the Properties of HVOF Cr₃C₂-NiCr Coatings, *Weld. World*, 1998, **41**, p 77-87
20. J.M. Guilemany, N. Espallargas, P.H. Suegama, A.V. Benedetti, and J. Fernández, High-Velocity Oxyfuel Cr₃C₂-NiCr Replacing Hard Chromium Coatings, *J. Thermal Spray Technol.*, 2005, **14**, p 335-341
21. M. Roy, A. Pauschitz, J. Bernardi, T. Koch, and F. Franek, Microstructure and Mechanical Properties of HVOF Sprayed Nanocrystalline Cr₃C₂-25(Ni20Cr) Coating, *J. Thermal Spray Technol.*, 2006, **15**, p 372-381
22. T.S. Sidhu, S. Prakash, and R.D. Agrawal, Characterizations and Hot Corrosion Resistance of Cr₃C₂-NiCr Coating on Ni-Base Superalloys in an Aggressive Environment, *J. Thermal Spray Technol.*, 2006, **15**, p 811-816
23. C.-J. Li, H. Yang, and H. Li, Effect of Gaseous Conditions on the Characteristics of HVOF Flame and Structure and Property of WC-Co Coatings, *Mater. Manuf. Process.*, 1999, **14**, p 383-395
24. G.-C. Ji, C.-J. Li, and Y.-Y. Wang, Microstructural Characterization of HVOF Sprayed Cr₃C₂-NiCr Coating, *Surf. Coat. Technol.*, 2006, **200**, p 6749-6757
25. Y. Arata, A. Ohmori, and C.-J. Li, Basic Study on Properties of Plasma Sprayed Ceramic Coatings, *Trans. Jpn. Weld. Res. Inst.*, 1986, **15**, p 339-348
26. P.A. Engel, *Impact Wear of Materials*. Elsevier Scientific Publishing Company, Amsterdam, 1976, p 80-113
27. C.-J. Li, K. Sonoya, G.-C. Ji, and Y.-Y. Wang, Effect of Powder Type on the Relationship Between Spray Parameters and Properties of HVOF Sprayed Cr₃C₂-NiCr Coatings. *Thermal Spray: Meeting the Challenges of the 21st Century*, C. Coddet, Ed., Materials Park, OH: ASM International, 1998, p 253-262
28. A. Ohmori and C.-J. Li, Quantitative Characterization of the Structure of Plasma Sprayed Al₂O₃ Coating by Using Copper Electroplating, *Thin Solid Films*, 1991, **201**, p 241-252
29. A. Ohmori, C.-J. Li, and Y. Arata, Influence of Plasma Spray Conditions on the Structure of Al₂O₃ Coatings, *Trans. Jpn. Weld. Res. Inst.*, 1990, **19**, p 259-270
30. C.-J. Li and A. Ohmori, The Lamellar Structure of a Detonation Gun Sprayed Al₂O₃ Coating, *Surf. Coat. Technol.*, 1996, **82**, p 254-258
31. C.-J. Li and A. Ohmori, Relationship Between the Structure and Properties of Thermally Sprayed Coatings, *J. Thermal Spray Technol.*, 2002, **11**, p 365-374
32. C.-J. Li, G.-J. Yang, and A. Ohmori, Relationship Between Particle Erosion and Lamellar Microstructure for Plasma Sprayed Alumina Coatings, *Wear*, 2006, **260**, p 1166-1172
33. Y.Y. Wang, Effect of the Spray Particle State on the Adhesive Strength of High Velocity Oxy-Fuel Sprayed Coating, Ph.D. Thesis, Xi'an Jiaotong University, 2001, p. 35-40
34. C.-J. Li, Y.Y. Wang, T. Wu, and G.C. Ji, Effect of Types of Ceramic Materials in Aggregated Powder on the Adhesive Strength of HVOF Cermet Coating, *Surf. Coat. Technol.*, 2001, **145**, p 113-120
35. G.-C. Ji, C.-J. Li, Y.-Y. Wang, W.-Y. Li, and G.-J. Yang, Method for Quantitative Evaluation of Carbide Loss During HVOF Spraying of Cr₃C₂-NiCr Coating, *Proceedings of the International Thermal Spray Conference*, B. Marple, M. Hyland, Y.-C. Lau, R. Lima, and J. Voyer, Eds., May 15-18, 2006 (Seattle, USA), ASM International, 2006